

## Improved performance of Differential Mobility Analyzers with 3D-printed flow straighteners

Loizidis, C.; Costi, M.; Lekaki, N.; Bezantakos, S.; Biskos, G.

**DOI**

[10.1016/j.jaerosci.2020.105545](https://doi.org/10.1016/j.jaerosci.2020.105545)

**Publication date**

2020

**Document Version**

Final published version

**Published in**

Journal of Aerosol Science

**Citation (APA)**

Loizidis, C., Costi, M., Lekaki, N., Bezantakos, S., & Biskos, G. (2020). Improved performance of Differential Mobility Analyzers with 3D-printed flow straighteners. *Journal of Aerosol Science*, 145, Article 105545. <https://doi.org/10.1016/j.jaerosci.2020.105545>

**Important note**

To cite this publication, please use the final published version (if applicable). Please check the document version above.

**Copyright**

Other than for strictly personal use, it is not permitted to download, forward or distribute the text or part of it, without the consent of the author(s) and/or copyright holder(s), unless the work is under an open content license such as Creative Commons.

**Takedown policy**

Please contact us and provide details if you believe this document breaches copyrights. We will remove access to the work immediately and investigate your claim.



## Technical note

## Improved performance of Differential Mobility Analyzers with 3D-printed flow straighteners

C. Loizidis<sup>a</sup>, M. Costi<sup>a</sup>, N. Lekaki<sup>a</sup>, S. Bezantakos<sup>a</sup>, G. Biskos<sup>a,b,\*</sup><sup>a</sup> Climate and Atmosphere Research Center, The Cyprus Institute, Nicosia, 2121, Cyprus<sup>b</sup> Faculty of Civil Engineering and Geosciences, Delft University of Technology, Delft, 2628CN, the Netherlands

## ARTICLE INFO

## Keywords:

Aerosol particle sizing  
Laminar flow  
Laminarizer

## ABSTRACT

The Differential Mobility Analyzer (DMA) is currently the most effective instrument for sizing sub-micrometer aerosol particles. An important requirement to ensure good performance in terms of sizing accuracy and resolution is that the flow field remains laminar and undisturbed along its classification zone. To achieve that, a flow straightener (or flow laminarizer) is employed at the sheath flow inlet, located at the top of the classification column. In this study, we assess the performance of a custom-made DMA using different sheath flow straighteners made out of plastic fabric materials or built by 3D printing. Our tests show that 3D-printed flow straighteners can achieve comparable, and in some cases better, results to those used in commercial DMAs (e.g., fine nylon meshes; Dacron®). Considering the great flexibility and ease in manufacturing offered by 3D printing, our findings show that this technology provides a promising alternative for building enhanced flow straightening systems.

## 1. Introduction

The Differential Mobility Analyzer (DMA; Knutson & Whitby, 1975) is undoubtedly one of the most effective instruments for sizing aerosol particles having diameters ranging from the nanometer scale and up to almost a micron. To achieve that, it combines a flow and an electrostatic field to classify particles based on their electrical mobility. While establishing a uniform electric field within the DMA classification column is relatively easy, doing so for the flow field can be rather challenging primarily because two flows (i.e., that carrying the aerosol particles and the particle-free sheath flow) are merged. Flow disturbances introduced when the two flows merge can cause local eddies and consequently deterioration of the DMA performance.

Despite that conventional cylindrical DMAs operate at relatively low Reynolds numbers (typically less than 400) and thus at laminar flow conditions, flow disturbances can be introduced i. at the point where the polydisperse aerosol inlet flow meets smoothly the sheath flow (Eichler, de Juan, & Fernandez de la Mora, 1998), and ii. by the way that the sheath flow is introduced at the top of the classification column. To minimize the effect of the former, the aerosol flow is typically maintained lower than ca. 10% of the sheath flow (Strattmann et al., 1997). For the latter, a flow straightener (FS), typically made out of a fine electrically insulating fabric mesh, is used to suppress lateral fluid velocity components induced by swirling motion. This can cause flow disturbances, while reducing substantially the length required for the development of a fully-developed velocity profile within the classification column.

The sheath flow in the classification zone of the DMA ensures that the particles will migrate from the outer to the inner electrode on

\* Corresponding author. Climate and Atmosphere Research Center, The Cyprus Institute, Nicosia, 2121, Cyprus.  
E-mail address: [g.biskos@cyi.ac.cy](mailto:g.biskos@cyi.ac.cy) (G. Biskos).

**Table 1**  
Characteristic details of all the tested FSs.

Flow Straightener	Pore Shape	Pore Size ( $\mu\text{m}$ )	Open Area (%)
Dacron® FS (fabric)	Square	90	31.6
FS#1 (fabric)	Asymmetric	153	36.6
FS#2 (fabric)	Asymmetric	63	18.9
FS#3 (fabric)	Square	160	52.9
FS#4 (fabric)	Square	35	27.3
FS#5 (fabric)	Square	27	16.2
FS#6 (3D-printed)	Square	1300	55.2
FS#7 (3D-printed)	Square	780	34.4
FS#8 (3D-printed)	Asymmetric	570	46.1
FS#9 (3D-printed)	Triangle	310	9.6

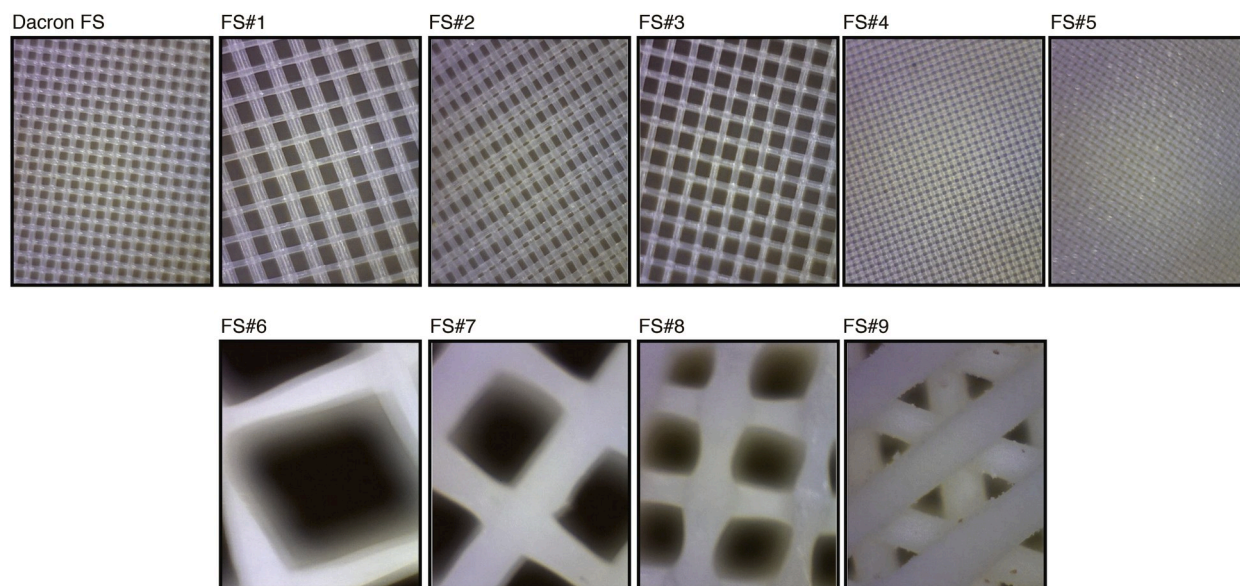


**Fig. 1.** Images of the tested flow straighteners determined by optical microscopy.

well-defined trajectories. Any flow disturbances within the DMA can induce small deviations from these trajectories, thereby affecting resolution of and particle transmission through the classifier as indicated by studies employing numerical models (e.g., [Chen & Pui, 1997](#)). Most DMAs (e.g., the commonly used TSI Model 3081 DMA) employ FSs made of a double layer of Dacron® nylon fabric. Here we investigate nine different FSs by testing how they affect the performance of a custom-made cylindrical DMA. Four of the FSs were 3D-printed using Acrylonitrile Butadiene Styrene (ABS), while the rest were made of different fabrics (small nylon meshes) including one made of Dacron® that was used as a reference. The effects of each FS on the performance of the DMA were evaluated by comparing the experimentally and theoretically determined transfer function of the instrument ([Stolzenburg, 2018](#)).

## 2. Experimental set-up and calculation methods

All flow straighteners had the same overall dimensions in order to fit in the test DMA, but differed in terms of material, pore size/shape and porosity as determined by optical microscopy (cf. [Table 1](#) and [Fig. 1](#); additional technical details, including a drawing of the 3D-printed FSs, are provided in the supplement). It should be noted here that in all the experiments a metallic perforated plate was also used at the bottom of the DMA to ensure flow uniformity at that end. The performance of each FS was assessed by experimentally determining the Transfer Function (TF) of the DMA (i.e., the function giving the probability of a particle of a given electrical mobility, or size, that enters the instrument, to exit through its monodisperse particle outlet) when that was operated under different operating conditions. The height of the TF corresponds to the maximum probability of particles entering the DMA to exit through the monodisperse particle outlet, whereas its Full Width at Half Maximum (FWHM) to the resolution of the DMA. Deviations from the theoretical TF ([Stolzenburg, 2018](#); cf. supplement for details), in terms of its height and its FWHM were then calculated for each FS and for each sheath flow rate tested.

The TF of the DMA used to test the different FSs was determined using a tandem DMA (TDMA) configuration ([Birmili et al., 1997](#)), as shown in [Fig. 2](#). In brief, polydisperse aerosol particles were generated by atomizing (through a TSI Model 3076 atomizer) a 0.5% w/v aqueous ammonium sulfate solution. The resulting droplets were then dried by passing them through a silica-gel diffusion drier,

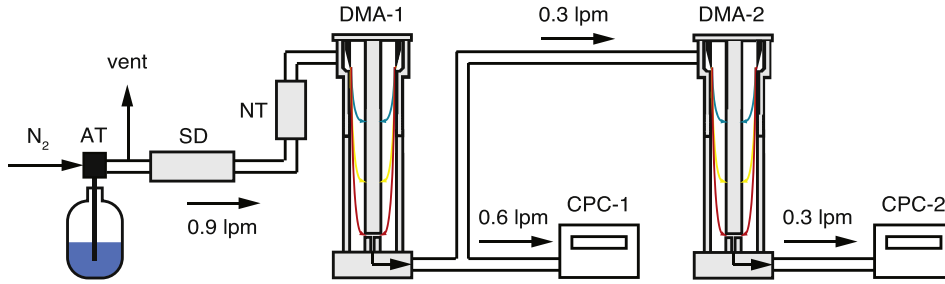


**Fig. 2.** Schematic layout of the experimental set-up used to determine the performance of the test DMA (i.e., DMA-2) when different FS were employed. Key: AT: Atomizer; SD: Silica-gel diffusion drier; NT: Aerosol charge neutralizer; DMA: Differential Mobility Analyzer; CPC: Condensation Particle Counter.

**Table 2**

Summary of the results reflecting the sizing accuracy of the test DMA (expressed as % difference between measured and predicted particle size selected by the DMA) when using different FSs.

Flow Straightener	Mobility Diameter Deviation (%)					
	3 lpm	6 lpm	9 lpm	13 lpm	20 lpm	
Dacron® FS (fabric)	2.7	3.2	3.8	2.0	1.6	
Without FS	3.6	4.8	5.9	–	–	
FS#1 (fabric)	1.3	1.9	2.1	–	–	
FS#2 (fabric)	2.1	2.6	3.2	–	–	
FS#3 (fabric)	2.3	2.9	3.5	2.4	2.3	
FS#4 (fabric)	3.4	3.7	3.9	2.9	2.8	
FS#5 (fabric)	4.2	4.7	5.3	2.1	1.8	
FS#6 (3D-printed)	2.6	2.6	0.7	1.2	–	
FS#7 (3D-printed)	2.1	2.5	2.3	0.1	4.5	
FS#8 (3D-printed)	3.2	3.8	1.6	–	–	
FS#9 (3D-printed)	3.0	3.3	3.9	1.6	0.9	

charge-neutralized by a  $^{85}\text{Kr}$ -source (TSI Model 3077A) aerosol neutralizer to an equilibrium distribution (Wiedensohler, 1988), and size-selected by the first DMA of the setup (DMA-1; custom-made DMA with characterized TF, operated at fixed voltage). A fraction of the monodisperse aerosol downstream DMA-1 was sampled by a first Condensation Particle Counter (CPC-1; TSI Model 3783) to measure the concentration of the particles, and the rest was used to characterize the performance of the test DMA (DMA-2 in the setup; custom-made DMA) operated in a stepping voltage mode and coupled with a second CPC (CPC-2; TSI Model 3025A). The DMAs used in this study are similar to those of standard DMAs manufactured by TSI. Their characteristic dimensions are provided in the supplement (cf. Table S1).

Both DMAs employed closed loop systems for the sheath flows, whereas the aerosol flow through the entire system was controlled by the two CPCs employed in the set-up, having sample flow rates of 0.6 (for CPC-1) and 0.3 (for CPC-2) lpm as shown in Fig. 2. As a result, a sample aerosol flow rate of 0.9 lpm was pulled through DMA-1 and 0.3 lpm through DMA-2. The sheath flow rate of DMA-1 was set to 9 lpm, in order to achieve an aerosol to sheath flow ratio of 1:10. The sheath flow rate of DMA-2 was varied from 3 to 20 lpm in order to test the performance of the FSs at different flow rates, yielding aerosol to sheath flow ratios that ranged from 1:10 to 1:67.

All tests were conducted using nearly monodisperse particles, selected by DMA-1, having a diameter of ca. 50 nm. Similarly to the approach followed by Giamarelou, Stolzenburg, Chen, and Biskos (2013) and Bezantakos, Giamarelou, Huang, Olfert, and Biskos (2016), a parametric version of the TF (cf. Eq. S18 in the supplement) was used to capture deviations between measurements and predictions (i.e., using the theoretical TF provided by Stolzenburg, 2018). The fitting parameters affect the TF in terms of its height and its width, thus making it possible to fit to the experimental observations (cf. supplement).

The measurements from the TDMA setup are related to the theoretical performance of the two DMAs as follows (Stolzenburg & McMurry, 2008):

$$\frac{N_2 \cdot CPC_{Ratio}}{N_1 \cdot P'} = \frac{\int_0^\infty \Omega_1(Z_p, Z_{p1}^*) \cdot \Omega_2(Z_p, Z_{p2}^*) \cdot dZ_p}{\int_0^\infty \Omega_1(Z_p, Z_{p1}^*) \cdot dZ_p} \quad (1)$$

Here,  $N_1$  and  $N_2$  are the measurements reported by CPC-1 and CPC-2, respectively,  $CPC_{Ratio}$  is a factor accounting for the potential mismatch of the two CPCs,  $P'$  is a function to correct the measurements for the diffusional losses in the tubing downstream DMA-1 (ca. 0.7 m long), whereas  $\Omega_1$  and  $\Omega_2$  are the transfer functions of DMA-1 and DMA-2, respectively. Equations for  $P'$ ,  $\Omega_1$  and  $\Omega_2$  are provided in the supplement.  $CPC_{Ratio}$  was experimentally determined to be ca. unity by sampling the same monodisperse aerosol flow out of DMA-1 for 20 min before every experiment and taking the ratio of the average values.

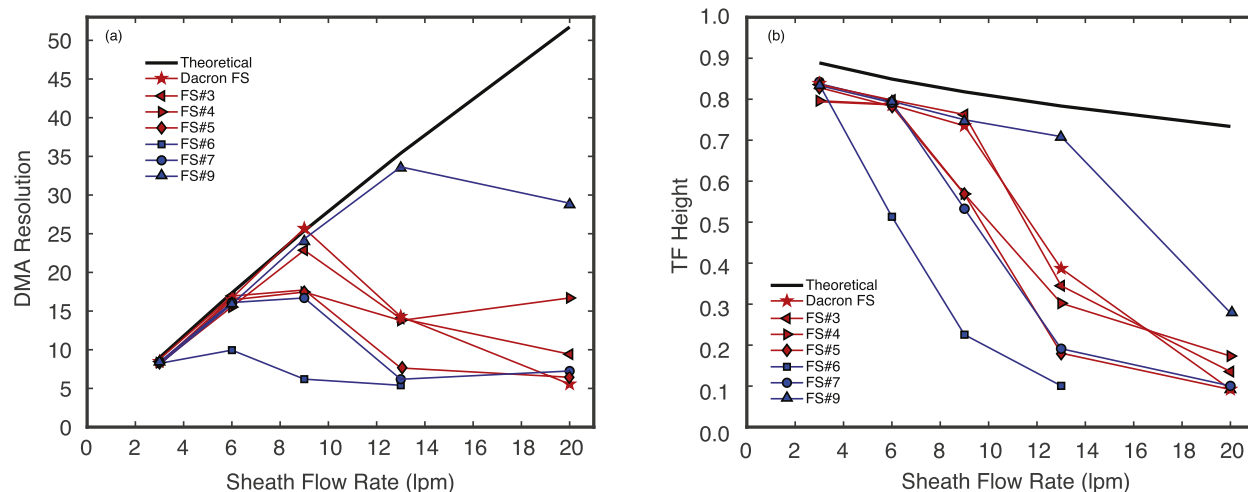


Fig. 3. DMA resolution (a) and TF height (b) of the test DMA (i.e., DMA-2 in the setup shown in Fig. 2) as a function of the sheath flow rate and when different FSs were employed.

In each TDMA experiment we obtain a set of  $N_1$  and  $N_2$  values, corresponding to the particle number concentrations measured downstream of DMA-1 and of DMA-2, respectively. Assuming that  $P'$  and  $CPC_{Ratio}$  remain constant throughout each experiment lasting for ca. 20 min, and that the TF of DMA-1 (i.e.,  $\Omega_1$  in Eq. 1) is constant and well-defined, the TF of DMA-2 (i.e.,  $\Omega_2$  in Eq. 1) is obtained by using a custom-made fitting algorithm (cf. supplement).

### 3. Results and discussion

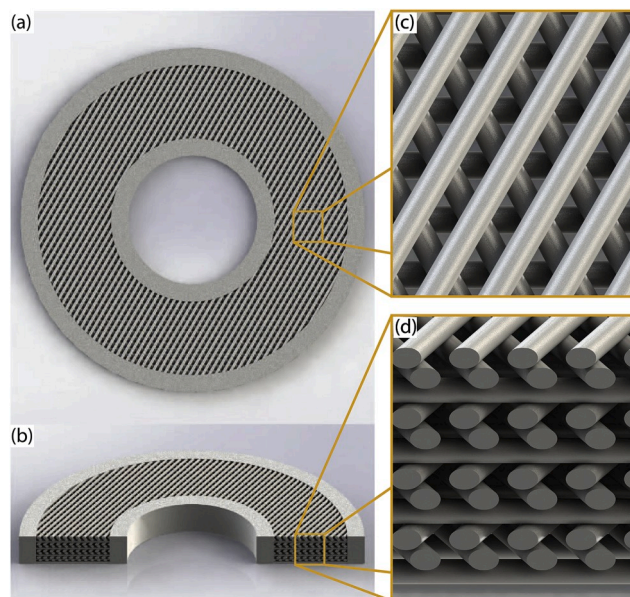
Table 2 shows the sizing accuracy of the tested DMA, determined as the % difference between predicted and measured mean particle size selected by the tested DMA when different FSs are employed. Interestingly, all FS yield a sizing accuracy within  $\pm 5\%$  under almost all tested conditions, whereas the performance of the DMA in terms of sizing the sample particles remains good even when no FS is used. This is not so surprising considering that the flow disturbances that are suppressed by the FSs are small, affecting mainly the resolution rather the sizing capability of the DMA.

Fig. 3 shows the resolution and the TF height of DMA-2 when different flows and FSs were used, in comparison to theoretical predictions. When DMA-2 is operated with a sheath flow of 3 and 6 lpm, almost all straighteners perform well, exhibiting deviations between theoretical and experimentally measured resolutions within  $\pm 10\%$ . The only exception is the 3D-printed FS having the largest pore size (i.e., 1.3 mm; FS#1), which resulted in a measured resolution that is 43% less than the theoretical when the sheath flow used in DMA-2 is 6 lpm. When the sheath flow rate is increased to 9 lpm, the only FSs yielding a resolution that is comparable to the theoretical are FS#9, which is 3D-printed, as well as FS#3 and the Dacron® FS. When the sheath flow is increased even further, the only FS that exhibits a good enough performance (i.e., at 13 lpm only 5% and at 20 lpm 44% less than the theoretically expected resolution) is FS#9, whereas the fabric straighteners exhibit significant deviations (more than 70%) from theory.

It should be noted here that all FSs tested in this work created a small step (ranging from 0.7 to 1.0 mm in height) between their outer boundary (for the 3D-printed), or rings (for the fabric), and the walls of the inside electrodes of the DMA. This was done following the design of the Dacron® FS that is used here as a reference, in order to ensure comparability. Such steps are known to deteriorate the resolution of the DMAs at high sheath flow rates, and are thus advised to be avoided (Fernandez de la Mora, Gao, & Perez-Lorenzo, 2017). Given that all the tested FSs created steps of very similar heights, however, make our results highly intercomparable and strengthen our conclusion that FS#9 attributes a performance to the DMA that is closer to that predicted by theory compared to the rest. Most importantly, even at the highest flow rate tested (i.e., 20 lpm), FS#9 outperforms the rest of the tested FSs, including the reference one made out of Dacron®.

Different FSs appear also to affect the height of the measured TF of DMA-2, especially at sheath flow rates approx. equal or larger than 6 lpm. More specifically only one of the 3D-printed FSs (i.e., FS#9) provided measurements that are comparable with theoretical predictions at sheath flow rates higher than 6 lpm. Fabric FSs having smaller pore size (i.e., FS#4 and FS#5 with pores sizes of 35 and 27  $\mu\text{m}$ , respectively) resulted in measured TFs with heights that are almost 30% less to those predicted by theory at 9 lpm of sheath flow. The Dacron® FS and FS#3, having pore sizes of 90 and 160  $\mu\text{m}$ , respectively, exhibited deviations between experimentally and theoretically determined TF heights that were respectively 10 and 7% less. At higher sheath flow rates (i.e., 13 and 20 lpm), however, those two fabric FSs resulted in a reduced, compared to the theoretical, TF height by more than 50%.

It should be noted here that the results obtained when no FS was used in DMA-2, as well as when FS#1, FS#2 and FS#8 (that had asymmetrical pore shapes) were employed, are not depicted in Fig. 3. They are provided in Table S2 of the supplement together with the results obtained when employing all the other FSs. Tested FSs having fabrics with asymmetrical pore shape (i.e., FS#1 and FS#2; cf. Fig. 1) resulted in significant degradation in the DMA performance even at 9 lpm sheath flow rate (cf. Table S2), despite that their



**Fig. 4.** Render illustrations of FS#9, including top view (a), 3D cross-sectional view (b), as well as zoomed in views of the top (c) and of the cross-section (d) of the porous part of the FS.

pore size was not much different than that of the other fabrics used in our tests.

Contrary to manufacturing FSs using fabrics, using 3D-printing offers the advantage of producing them in a single step. In addition, it provides great flexibility in using different design patterns, which in turn affects the overall performance of the FSs. This is demonstrated with FS#9, which uses a multilayer array of threads that result in triangular pores as shown in Fig. 4, differing from those that are commonly employed in FSs in most DMAs (i.e., rectangular). Evidently, DMA-2 exhibits the best performance for all flow conditions tested in this work when employing FS#9. A possible explanation for this observation is that the triangular shape pattern of this FS, is the closest to the honeycomb structure, which is very effective at reducing lateral flow turbulence (Scheiman & Brookst, 1981). Another plausible explanation is that FS#9 has a multi-layer structure, providing a significantly longer laminarization path compared to the other FSs investigated here.

The good performance of the DMA when using FS#9, which was better even from the case when the reference Dacron® FS was employed at sheath flow rates up to 20 lpm, warrants for further investigating the use of 3D-printed straighteners to run conventional and/or low-cost DMAs (Barmounis, Maisser, Schmidt-Ott, & Biskos, 2015) at substantially higher sheath flow rates (e.g., up to 20 lpm) or with high-flow DMAs (Fernández de la Mora & Kozlowski, 2013). For the latter, which are used for classifying nanoparticles (Wang et al., 2014) and even atomic clusters (Maisser, Barmounis, Attoui, Biskos, & Schmidt-Ott, 2015) with high resolution, flow laminarization is rather important, typically requiring an additional pre-laminarization stage (Amo-Gonzalez & Pérez, 2018).

In summary, the measurements reported in this work show that 3D printing can be used to manufacture flow straighteners that exhibit better performance compared to traditional systems made of nylon fabrics. This has been verified by assessing deviations between the measured and the theoretical transfer function of a custom-made DMA employed in the tests. Interestingly, the 3D-printed straightener, having a triangular pore shape combined with a high surface density and larger pores compared to the other FSs investigated here, attributed to the test DMA a performance that compared better with theory. Considering the flexibility and ease of manufacturing of 3D printing, our results show that employing this technology to build flow straightness for DMAs, can improve their performance and thus is a better alternative compared to existing practices.

## Acknowledgements

This work was co-funded by the European Regional Development Fund and the Republic of Cyprus through the Research Promotion Foundation (Projects: EXCELLENCE/1216/0492 and POST-DOC/0916/0287).

## Appendix A. Supplementary data

Supplementary data to this article can be found online at <https://doi.org/10.1016/j.jaerosci.2020.105545>.

## References

- Amo-Gonzalez, M., & Pérez, S. (2018). Planar differential mobility analyzer (DMA) with resolving power of 110. *Analytical Chemistry*, 90(11), 6735–6741.
- Barmounis, K., Maisser, A., Schmidt-Ott, A., & Biskos, G. (2015). Lightweight differential mobility analyzers: Towards new and inexpensive manufacturing methods. *Aerosol Science & Technology*, 50, ii–v.
- Bezantakos, S., Giamarelou, M., Huang, L., Olfert, J., & Biskos, G. (2016). Modification of the TSI 3081 differential mobility analyzer to include three monodisperse outlets: Comparison between experimental and theoretical performance. *Aerosol Science & Technology*, 50(12), 1342–1351.
- Birmili, W., Stratmann, F., Wiedensohler, A., Covert, D., Russell, L. M., & Berg, O. (1997). Determination of differential mobility analyzer transfer functions using identical instruments in series. *Aerosol Science & Technology*, 27, 215–223.
- Chen, D.-R., & Pui, D. Y. H. (1997). Numerical modeling of the performance of DMAs for nanometer aerosol measurement. *Journal of Aerosol Science*, 28, 985–1004.
- Eichler, T., de Juan, L., & Fernandez de la Mora, J. (1998). Improvement of the resolution of TSI's 3071 DMA via redesigned sheath air and aerosol inlets. *Aerosol Science & Technology*, 29(1), 39–49.
- Fernandez de la Mora, J., Gao, P., & Perez-Lorenzo, L. J. (2017). Eliminating the main source of instability and turbulence in TSI's 3071 DMA. *Aerosol Science & Technology*, 51(7), 896–902.
- Fernández de la Mora, J., & Kozlowski, J. (2013). Hand-held differential mobility analyzers of high resolution for 1–30nm particles: Design and fabrication considerations. *Journal of Aerosol Science*, 57, 45–53.
- Giamarelou, M., Stolzenburg, M. R., Chen, D.-R., & Biskos, G. (2013). Comparison between the theoretical and experimental performance of a differential mobility analyzer with three monodisperse-particle outlets. *Aerosol Science & Technology*, 47, 406–416.
- Knutson, E. O., & Whitby, K. T. (1975). Aerosol classification by electric mobility: Apparatus, theory and applications. *Aerosol Science & Technology*, 6, 443–451.
- Maisser, A., Barmounis, K., Attoui, M. B., Biskos, G., & Schmidt-Ott, A. (2015). Atomic cluster generation with an atmospheric pressure spark discharge generator. *Aerosol Science & Technology*, 49, 886–894.
- Scheiman, J., & Brookst, J. D. (1981). Comparison of experimental and theoretical turbulence reduction from screens, honeycomb, and honeycomb – screen combinations. *Journal of Aircraft*, 18(8), 638–643.
- Stolzenburg, M. R. (2018). A review of transfer theory and characterization of measured performance for differential mobility analyzers. *Aerosol Science & Technology*, 52(10), 1194–1218.
- Stolzenburg, M. R., & McMurry, P. H. (2008). Equations governing single and tandem DMA configurations and a new log-normal approximation to the transfer function. *Aerosol Science & Technology*, 42(6), 421–432.
- Stratmann, F., Kauffeldt, T., Hummes, D., & Fissan, H. (1997). Differential electrical mobility analysis: A theoretical study. *Aerosol Science & Technology*, 26(4), 368–383.
- Wang, Y., Fang, J., Attoui, M., Chadha, T. S., Wang, W.-N., & Biswas, P. (2014). Application of Half Mini DMA for sub 2 nm particle size distribution measurement in an electrospray and a flame aerosol reactor. *Journal of Aerosol Science*, 71, 52–64.
- Wiedensohler, A. (1988). An approximation of the bipolar charge distribution for particles in the submicron size range. *Journal of Aerosol Science*, 19, 387–389.